

# Frontiers in structured illumination microscopy

FLORIAN STRÖHL AND CLEMENS F. KAMINSKI\*

Department of Chemical Engineering and Biotechnology, University of Cambridge, Pembroke Street, CB2 3RA Cambridge, UK

\*Corresponding author: cfk23@cam.ac.uk

Received 2 February 2016; revised 5 April 2016; accepted 13 April 2016 (Doc. ID 258778); published 15 June 2016

At the start of this millennium, the principles of structured illumination microscopy (SIM) had been established and the concept of resolution doubling demonstrated experimentally in two dimensions. Breathtaking advances have since taken place, making SIM one of the most powerful and versatile superresolution methods available today, routinely used in the study of biochemical processes in laboratories around the world. In theory there is no inherent limit to the resolution obtainable with certain modalities of SIM, and new variants have the potential to operate at even higher speeds and sensitivity than currently realized. In this review, we focus on the very latest innovations in SIM theory and practice, which are set to continue the revolution of this method into the future. Examples include confocal implementations of the SIM principle, which can be used in combination with two-photon excitation and adaptive optics. We present recent applications of such approaches in the life sciences, which illustrate their potential to revolutionize intravital research, by providing the ability to watch life at the molecular scale, at high speeds, and deep within living organisms. A different variant makes use of standing plasmonic waves or localized surface plasmons to confer performance enhancements to 2D SIM modalities. Research on these latter techniques is in its infancy but already shows great potential for their development into powerful *in vitro* probes for chemical processes at solid/liquid interfaces. Physical concepts are reviewed in detail, and future directions are presented along which the field might fruitfully develop, holding promise for new discoveries on the molecular scale.

Published by The Optical Society under the terms of the [Creative Commons Attribution 4.0 License](#). Further distribution of this work must maintain attribution to the author(s) and the published article's title, journal citation, and DOI.

**OCIS codes:** (180.2520) Fluorescence microscopy; (100.6640) Superresolution; (110.6880) Three-dimensional image acquisition; (250.5403) Plasmonics.

<http://dx.doi.org/10.1364/OPTICA.3.000667>

## 1. INTRODUCTION

*Breaking the diffraction limit.* The field of superresolution microscopy, so-called optical nanoscopy, has been recognized recently with the award of the Nobel Prize in Chemistry to the inventors of stimulated emission depletion microscopy (STED) [1] and single molecule localization microscopy (SMLM) [2,3]. The winners, Stefan Hell, William Moerner, and Eric Betzig, were among the first to recognize that the classical resolution barrier in optical microscopy, formulated almost 150 years ago by Ernst Abbe [4,5], can be overcome by exploiting mechanisms that control the switching of fluorophores between fluorescent on and off states. STED achieves this by depleting fluorescence in the periphery of a confocal excitation beam via stimulated emission. In SMLM, physical or chemical methods are used to control the number of fluorophores that are in the on state, such that only a sparse subset is imaged at any one time; hence images from individual fluorophores can be discriminated spatially on wide-field detectors. SMLM achieves superresolution via the precise localization of individual molecules from their emission patterns, and many variants exist today that are based on this principle [6]. Notable examples include photoactivated localization microscopy (PALM) [7], fluorescence PALM [8], stochastic optical reconstruction

microscopy (STORM) [9], and direct STORM [10], with the latter also known as ground state depletion microscopy followed by individual molecule return [11]. In parallel with these developments, structured illumination microscopy (SIM) was developed as an alternative means to achieve optical superresolution, and today SIM has evolved into one of the most powerful and versatile optical superresolution techniques available, combining resolution improvement with good acquisition speed and flexibility of use. In principle, any fluorophore that can be imaged in wide-field fluorescence microscopes is amenable to interrogation by a SIM microscope, and thus the complete catalog of fluorescence probes that has been developed for biochemical analysis is available for the method. Unsurprisingly, the field has seen extraordinary development over the last decade, and many SIM implementations have been reported since the early pioneering works by Sheppard [12], Heintzmann and Cremer [13], and Gustafsson [14]. The evolution of SIM and the rapid pace of its technical development have been documented in several excellent review articles. General overviews on optical nanoscopy methods usually include a discussion of SIM in addition to STED and SMLM techniques, and thus permit a comparison of respective features/advantages/disadvantages; examples include the review by Lippincott-Schwartz and Manley,

which provides a historical context for the development of the field as a whole [15]; and reviews by Hell [16] and Schermelleh [17], which compare the physical principles of various nanoscopy methods. The fundamental criteria for achieving superresolution in continuously labeled samples are lucidly discussed by Heintzmann and Gustafsson [18], and this is particularly relevant to SIM and to the conceptually related STED technique, which also makes use of a structured illumination pattern. Reviews specifically focused on SIM also exist that cover the technique in varying degrees of technical detail [19,20]. An outstanding and comprehensive review of the physical principles of SIM, its practical implementation, and mathematical derivations for SIM algorithms was recently published by Wicker [21]. A number of other reviews take a user perspective on the field, and cater to the needs of biologists, chemists, and other users of superresolution microscopy. Which technique is the most useful for my fast-moving sample [22]? Which techniques offer the best compromise between spatiotemporal resolution and 3D imaging capability [23]? What superresolution methods are available for cell biologists [24], and how are they applied in an optimal fashion [25]? How would SIM perform in the study of neuronal processes [26]? In light of these and similar publications that have appeared in the field, one may wonder where the need lies for yet another review on the topic of SIM. However, the underpinning technologies and theoretical methods are advancing at a phenomenal pace, and SIM is beginning to make an impact when used in conjunction with other imaging modalities as well, e.g., light sheet imaging [27]. Current reviews consider SIM mainly as a wide-field technique that utilizes two-beam [13,28,29] or three-beam [30,31] interference to generate sinusoidal illumination patterns. Here we follow a different approach and focus on the process of spatial frequency mixing as the fundamental principle that links traditional SIM and all its more recent variants. Hence, using the same conceptual approach, it is

possible to understand the physics of spot-scanning SIM, SIM on plasmonic substrates, and combinations of SIM with other imaging modalities, such as lattice light-sheet microscopy. The emphasis is on the fundamental principles of the technique, followed by the presentation of the latest innovations and applications of the technique in biomedical research. SIM is no longer restricted to sinusoidal excitation patterns and the imaging of thin samples at moderate speeds with moderate resolution improvements. The purpose of this mini review is thus also to give researchers an introduction to where this rapidly developing field is heading, and to provide enough conceptual background for scientists to start developing their own variants of SIM for their research.

## 2. PRINCIPLE OF SPATIAL FREQUENCY MIXING FOR SUPERRESOLUTION

Structured illumination techniques overcome limitations imposed by optical diffraction by encoding structural details corresponding to high spatial frequencies in the sample in low-frequency signals via spatial frequency mixing. Thus information can be recovered from low-frequency data that is otherwise lost by conventional imaging through an optical microscope. The spatial frequency bandwidth that can be transmitted through an objective is described by the optical transfer function (OTF), which supports spatial frequencies only up to a certain cutoff frequency  $k_c$ . In mathematical terms, information at spatial frequencies greater than  $k_c$  is weighted to zero. The OTF is the Fourier transform  $H(k)$  of the so-called point spread function (PSF) which is also known as the impulse response function of the imaging system,  $h(x)$ . SIM delivers better resolution than conventional microscopy by shifting high spatial frequencies into the accessible pass-band of the OTF, and can thus be viewed as a method that "increases the OTF support" (see Fig. 1).

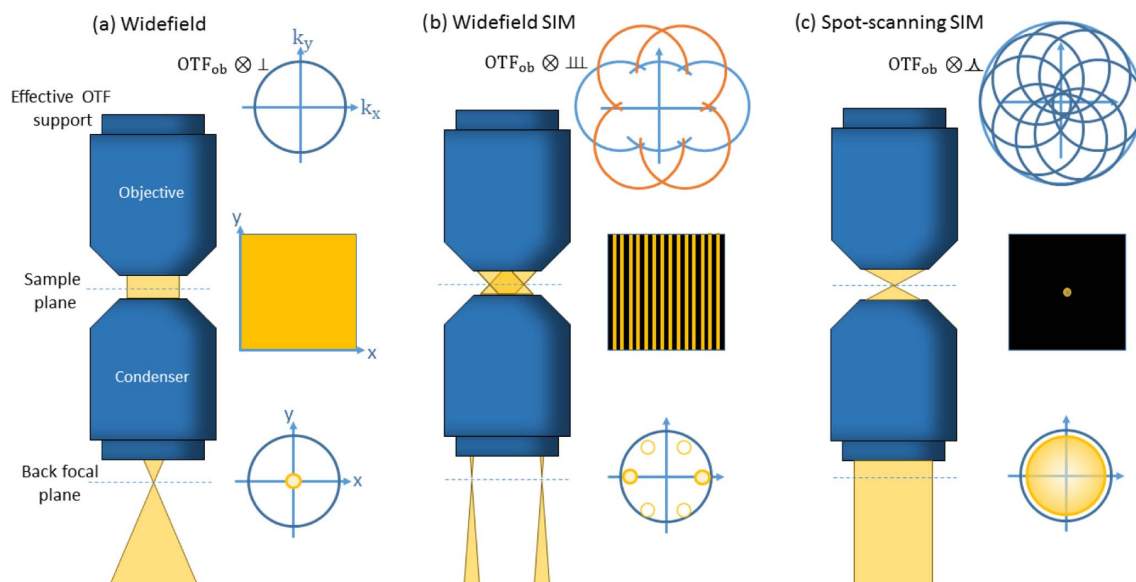


**Fig. 1.** Illumination modes in (a) wide-field imaging, (b) wide-field SIM, and (c) spot-scanning SIM. (b) In wide-field SIM, two laser beams illuminate the back focal plane of the condenser lens to form an interference pattern in the sample plane. Placing the foci of the illumination beams close to the periphery of the entrance pupil of the illumination condenser generates an illumination pattern with high spatial frequency on the sample; the higher this frequency, the better the achievable resolution. The effective OTF is then a convolution of the objective OTF and the spatial frequency spectrum of the illumination pattern (three delta functions). (c) The same principle holds true for spot-scanning SIM. Here, the back focal plane of the objective is filled completely with illumination light, thus producing a diffraction-limited spot in the sample plane. The spatial frequency content of the effective OTF is again the convolution of the spatial frequency content in the illumination pattern and the objective's OTF. (a) In wide-field imaging, this convolution is performed with a delta function; i.e., the OTF support is not increased.

The conventional wide-field implementation of SIM uses a sinusoidal light pattern excitation, which is formed by the interference of two laser beams on the sample [see Fig. 1(b)]. This pattern can be expressed as  $e(x) = 1 + \cos(k_e x)$ , and it leads to a fluorescent response in the sample, which can be modeled by the multiplication of the sample structure  $s(x)$  with the excitation pattern  $e(x)$ . The final image,  $i(x)$ , that is projected onto the camera is then blurred by the PSF, denoted by  $h(x)$ . The coordinate  $x$  refers to the nominal sample coordinate system, and the magnification of the system is neglected:

$$i(x) = [s(x) \times e(x)] \otimes h(x). \quad (1)$$

Blurring is modeled via the convolution operation  $\otimes$ . The accessible frequency content that is contained in the image, i.e., the achievable resolution, is obtained from the Fourier transform of Eq. (1):

$$I(k) = [S(k) \otimes E(k)] \times H(k). \quad (2)$$

Here capital letters denote the Fourier transforms of the respective real-space functions in Eq. (1). The variable  $x$  in real space becomes the spatial frequency variable  $k$  in Fourier space. Note that the blurring by the PSF in real space is denoted by a convolution operation in Eq. (1) and becomes a multiplication operation with the OTF in frequency space, as is evident from Eq. (2). Similarly, the multiplication of illumination and sample structures becomes a convolution, i.e., the sample information is "smeared across frequency space" by the Fourier transform of the excitation pattern. In conventional wide-field SIM the excitation pattern  $e(x)$  is sinusoidal with a spatial frequency  $k_e$ . Its Fourier transform  $E(k)$  thus purely consists of delta pulses.  $I(k)$  thus becomes

$$\begin{aligned} I(k) &= \left[ S(k) \otimes \left( \delta(k) + \frac{1}{2}\delta(k - k_e) + \frac{1}{2}\delta(k + k_e) \right) \right] \times H(k) \\ &= \left[ S(k) + \frac{1}{2}S(k - k_e) + \frac{1}{2}S(k + k_e) \right] \times H(k). \end{aligned} \quad (3)$$

This shows the essence of SIM: convolution with  $E(k)$  results in a shifting of the sample information to new frequency positions centered at  $\pm k_e$ . Although the result of this convolution operation is still curtailed by the OTF  $H(k)$ , it does now contain higher spatial frequency content, up to the sum of excitation and cutoff frequencies:  $k_{\text{SIM}} = k_e + k_c$ . It is important to note that this principle holds for any illumination pattern that contains high spatial frequencies, for example the illumination spot in a confocal microscope. Figure 1(c) demonstrates that a single diffraction-limited spot  $h_{\text{ex}}(x)$  contains all spatial frequencies up to the cutoff frequency of the condenser objective, and can thus in principle give rise to resolution doubling as well. In a scanning microscope this resolution is affected by the size of the detection pinhole, or, to be precise, the effective detector size [32]. As shown in Fig. 2, a conventional confocal microscope is only capable of increasing resolution if the pinhole of the setup is closed down to a very small aperture. This can be understood if one considers a single fluorophore, i.e., a point emitter  $\delta(x)$ , that is scanned by a diffraction-limited beam in the form of the excitation PSF  $h_{\text{ex}}(x)$  and imaged through an objective with impulse response  $h_{\text{det}}(x)$  onto a detector of spatial dimensions  $D(x)$ :

$$i(x) = [h_{\text{ex}}(x) \otimes \delta(x)] \times [h_{\text{det}}(x) \otimes D(x)]. \quad (4)$$

When the detector is infinitesimally small, i.e.,  $D(x) \sim \delta(x)$ , one obtains an effective PSF that is given by  $h_{\text{ex}}(x) \times h_{\text{det}}(x)$ , and this offers superresolution, since this product has a narrower distribution than either  $h_{\text{ex}}(x)$  or  $h_{\text{det}}(x)$  alone. This enhancement is lost if the detector has an extended area: for example, for an infinitely large detector, we have  $D(x) = 1$ , and the effective PSF is then

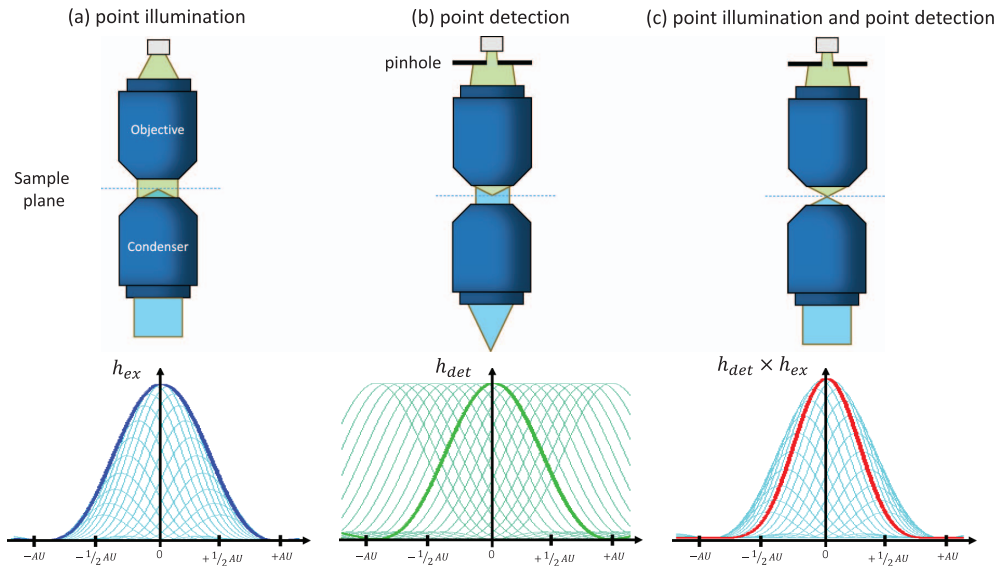


**Fig. 2.** PSF in a confocal microscope. Depending on the setup of a confocal microscope, its resolving power changes as described by Eq. (4). (a) If a diffraction-limited spot is illuminated but all of the generated fluorescence is imaged onto a large photodiode (convolution with  $D(x) \approx 1$ ), the resulting resolution is the PSF of the excitation light. (b) If the whole sample is illuminated but only a tiny part of the fluorescence is transmitted onto the detector—the rest is blocked by a pinhole—then the resolution as defined by the detection PSF is achieved. (c) Combining both point illumination and point detection with a tiny pinhole offers doubled resolution in the form of a confocal PSF that is the multiplication of the excitation and detection PSF. AU, Airy unit.



degraded to the excitation PSF  $h_{\text{ex}}(x)$ , as is evident from Eq. (4). It is worth adding a detail to this discussion that is often missed: even in the case of a fully opened pinhole (i.e., “no pinhole”), confocal microscopy confers a (modest) resolution enhancement over wide-field microscopy. This is because of the fluorescence Stokes shift, which means that the excitation PSF  $h_{\text{ex}}(x)$  is always smaller than the emission PSF  $h_{\text{det}}(x)$ . Resolution doubling by frequency mixing is, however, only achievable when a small pinhole is used.

Unfortunately, this superresolution potential is not accessible in practice due to the extremely low SNR in confocal microscopy when the pinhole is almost closed and the number of photons reaching the detector is severely restricted. Already, in 1988, Sheppard proposed an idea to overcome this problem in what we want to term spot-scanning SIM [12]. Through the use of a detector array composed of a multitude of small light-sensitive elements, each effectively acting as a pinhole, and using a post-processing step to assign photons detected at the different detector elements to their point of origin, he demonstrated that in principle superresolution is achievable with no loss of signal intensity. The concept was implemented experimentally more than 20 years later by Müller and Enderlein [33], who termed the method image scanning microscopy (ISM). In the next section we focus on this class of superresolution methods and recent developments.

### 3. SPOT-SCANNING SIM

In ISM resolution doubling is achieved, as in confocal microscopy, with an almost closed pinhole, but without the associated trade-off in signal-to-noise ratio (SNR). This is achieved by replacing the point detector in a conventional confocal microscope with a detector array, e.g., a CCD chip, and thus the 2D photon distribution of the signal, i.e., the PSF, is sampled. Each detector pixel can now be considered to be an independent point detector, with the pixel size representing a tiny confocal aperture. Every pixel thus records an independent superresolved image of the illumination point; however, it is shifted by roughly an amount of  $x/2$ , where  $x$  is the distance of the pixel from the image axis. A straightforward approach of summing all these images would re-create the image recorded by a conventional confocal microscope with the pinhole fully opened, as seen in Fig. 2(a). Shifting the information of each pixel to align the recorded data increases the overall SNR tremendously and even increases the resolution [34]. A rigorous analysis of the extent of this operation, image shifting, was recently provided by Sheppard *et al.* [35]. Thus, shifting the data from all individual pixels onto the optical axis before summing them up retains and even surpasses the superresolution capability of confocal microscopy, but with the benefit of a vastly increased SNR. In fact, the method has resolution-doubling capability in not only the lateral but also the axial direction, as explained in detail by Schulz *et al.* [36]. In practice, a 2D image is recorded on the detector array at each scan position of the excitation beam, and the recorded PSF is then either computationally scaled down or mapped onto an image grid that is scaled up by a factor of 2. The first ISM microscope by Müller and Enderlein used the “PSF shrinking approach” [33]—they scanned a diffraction-limited excitation beam across the sample and recorded the blurred fluorescence spots one by one on a camera. In a postprocessing step the acquired images were scaled and placed at the corresponding beam positions. With this procedure they proved the concept proposed

by Sheppard and the ability of confocal SIM to improve resolution. They also stated the advantage of providing optical sectioning that is inherent to confocal imaging. The big drawback, however, was the enormous number of raw images required for the method. For instance, to achieve a superresolved image of a  $10\ \mu\text{m} \times 10\ \mu\text{m}$  field of view, some 625,000 raw images were required, with an associated recording time of approximately 10 min. An obvious approach to speed up the method is to parallelize the acquisition process—and this is exactly what York *et al.* achieved in their variant of the method, termed multifocal SIM (MSIM) [37]. Here a digital micromirror device projects a 2D spot pattern onto the sample and hence collects spot data from hundreds of excitation spots simultaneously. The postprocessing of the data is analogous to that of ISM by Müller and Enderlein. In some cases this processing procedure can lead to artifacts in the final image, and therefore more robust reconstruction methods have been developed recently [38]. The technique enabled 3D imaging of live cells at frame rates reaching up to 1 Hz. Schulz *et al.* [36] presented a different parallelization approach by integrating ISM into a confocal spinning disk microscope. A conceptual variation is to perform the shifting and scaling operations required in spot-scanning SIM optically [39,40]. This offers the potential to greatly increase acquisition speed and to reduce the need for complex postprocessing of large image data sets. Collectively, these methods can be called optical photon reassignment microscopy (OPRA). Superresolution is achieved in OPRA by shrinking the illumination spot optically using an inverted telescope arrangement and by reassigning it to the appropriate camera position using a beam-scanning unit for the emission signal in addition to that required for excitation. This approach provides a speed enhancement over the original digital implementation of ISM and offers acquisition speeds reaching 0.5 Hz. Although MSIM is faster than these early implementations of ISM and OPRA, recent implementations of single-beam spot-scanning SIM can reach up to 13 frames per second [41], limited now by excitation saturation. However, all-optical versions of MSIM also exist. These methods were pioneered by York *et al.* [34] and are called instant SIM (iSIM), and currently represent the fastest SIM modalities reported. In iSIM a multitude of illumination spots are generated and emission patterns are scaled and shifted using microlens arrays that are scanned across the sample. Overall, this implementation provides frame rates of over 100 Hz with resolution doubling in three dimensions and in multiple colors [34]. Figure 3 provides a conceptual overview of the different spot-scanning techniques discussed in this section. It is worth noting that the all-optical implementations of spot-scanning SIM, namely iSIM [34], OPRA [40], and re-scan confocal microscopy [39], were all developed independently.

Impressive examples of the capabilities of iSIM include the ultrafast imaging of the rapid movement of motor-driven organelles in human lung fibroblasts, which traffic at speeds of up to  $1\ \mu\text{m s}^{-1}$ , and the visualization of the cytoskeleton within blood cells circulating deep in a living 3 day old zebrafish embryo [34]. Similarly, York *et al.* visualized fast contractions occurring in the endoplasmic reticulum in living cells [34], as shown in Fig. 4. These are remarkable developments of microscopy, and applications that would have been unthinkable not long ago. Wide-field implementations of SIM that use sinusoidal illumination patterns achieve less than one-tenth of these frame rates but offer better

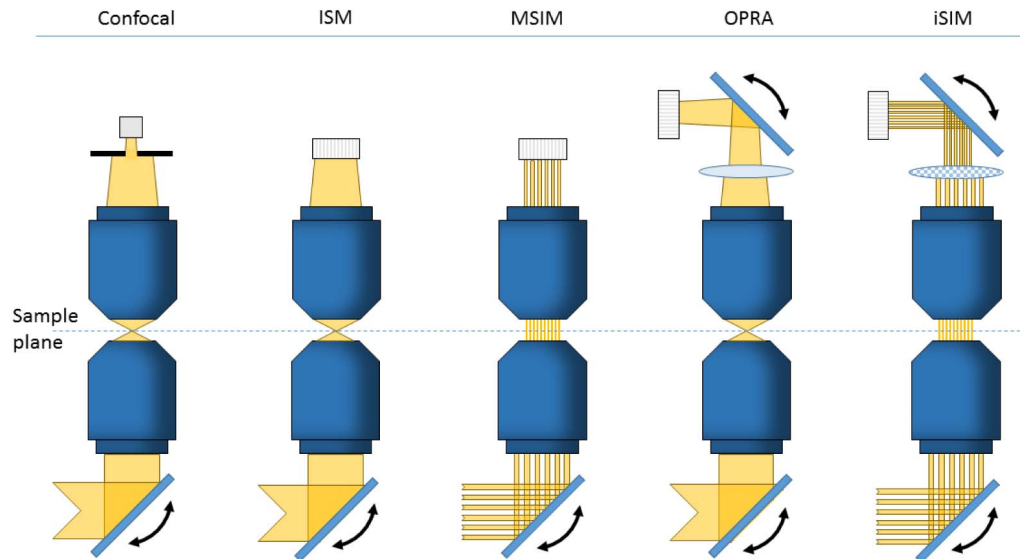


**Fig. 3.** Comparison of spot-scanning SIM techniques. In a conventional scanning confocal microscope, superresolution can only be achieved if a small pinhole is used [12], which is not practicable due to low signal levels in this case. In ISM [33], the point detector is replaced by a detector array to capture the entire shape of the excitation spot for each scan position in an individual image and process those images accordingly. In MSIM [37], the long acquisition time (10 min) of ISM is decreased via heavy parallelization of the imaging process, boosting frame-rates **1000-fold**. OPRA [40] is an all-optical implementation of ISM in the sense that all the postprocessing is done on the fly using **additional lenses and scanner units** to produce a superresolved image directly on the camera. Due to the limited speed of the scanners, the frame rate of OPRA is limited to 0.5 frames per second [39]. This limit can be overcome, similar to MSIM, via parallelization: the respective technique is called instant SIM, or iSIM [34,42]. This technique can provide imaging rates of over 100 frames per second through the use of multifocal illumination patterns in combination with microlens arrays for analogue processing in superresolution, and can thus outperform other SIM modalities in terms of imaging speed.

**SNR at high spatial frequencies** in return. Spot-scanning SIM, on the other hand, has the potential to confer performance advantages for **imaging in thicker samples or inside live tissue**. This is because the patterns that have to be projected in wide-field excitation degrade quickly with depth because of scattering and absorption. Furthermore, sinusoidal illumination patterns are usually generated by interfering two light beams that pass through high-NA objectives in the fashion shown in Fig. 1(b),

under conditions that offer only a very shallow working depth. Confocal spot-scanning techniques do not suffer from the latter problem, and they are, furthermore, highly compatible with adaptive optics techniques to correct for optical aberrations. Finally, spot scanning is compatible with two-photon excitation schemes, and thus inherently less affected by scattering in deep tissue. The advantages of two-photon excitation were described already in the '90s by Denk *et al.* [43]; here two photons whose combined

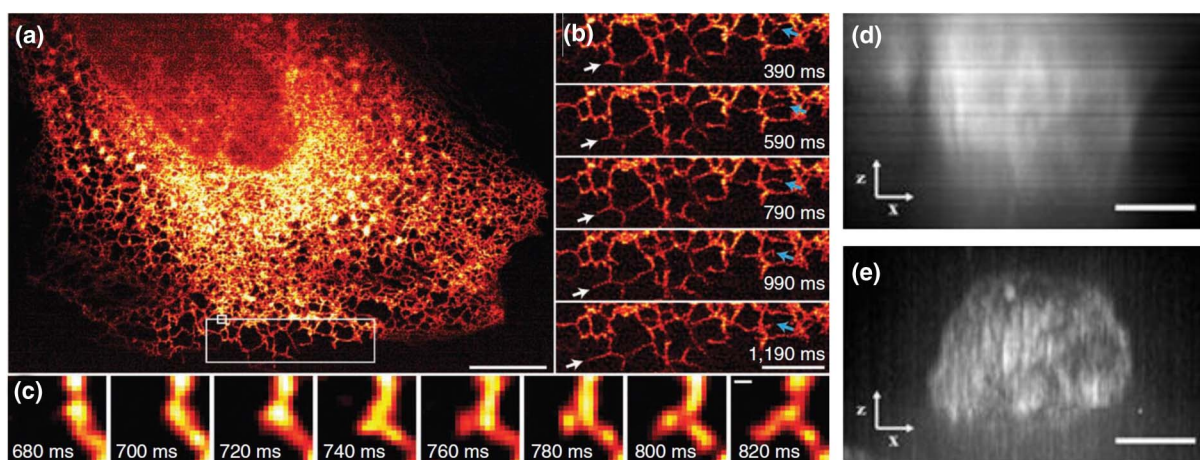


**Fig. 4.** Superresolution imaging, deep and fast. (a)–(c) iSIM is the fastest SIM technique to date (to our knowledge) and was used here to unveil the dynamics of the endoplasmic reticulum in human lung fibroblasts at frame rates of 100 Hz. The images reveal the rapid polymerization and depolymerization of the microtubule constituting the endoplasmic reticulum scaffold, revealing details that had been invisible before the advent of iSIM. Scale bars are 10  $\mu\text{m}$ , 5  $\mu\text{m}$ , and 200 nm, respectively. (d), (e) For deep tissue imaging, two-photon MSIM can be used, which enhances both resolution and, importantly, contrast when compared to conventional wide-field imaging. Shown is the salivary gland of a *Drosophila melanogaster* imaged (d) in wide-field and (e) by two-photon MSIM [44] in  $x$ - $z$  view (Scale bar 5  $\mu\text{m}$ ), imaged at 40  $\mu\text{m}$  depth in the sample. Reprinted by permission from Macmillan Publishers Ltd: [Nature Methods] [34] copyright (2013) and from Ingaramo *et al.* [44].

energy matches the optical transition are absorbed simultaneously, but the nonlinear intensity dependence of the process restricts absorption to a highly confined volume in the focal spot of the beam. This vastly reduces the generation of signal outside the illumination focal plane, and associated photobleaching in front of and behind the focal plane [43] is reduced. The method thus provides automatic sectioning capability.

To date, two variants of spot-scanning SIM have been implemented in a two-photon configuration: MSIM [44] and OPRA [45]. Using two-photon MSIM, it was possible to achieve a 145 nm resolution laterally and 400 nm resolution axially at imaging depths in live specimens exceeding 100  $\mu\text{m}$  and at frame rates of 0.2 Hz [44]. These impressive results could even be surpassed through use of two-photon OPRA; Winter *et al.* achieved frame rates of 1 Hz at comparable penetration depths. The speed of OPRA is limited by the pixel dwell time, while the speed of MSIM is restricted by the camera readout time. A combination of both techniques, multifocal two-photon SIM with all-optical processing, has yet to be demonstrated but offers exciting potential to become the new “gold standard” in thick tissue imaging *in vivo*: the parallelized approach compensates for pixel dwell times and limitations in readout speed, since on the fly all-optical processing obviates the need for multiple acquisitions to generate superresolved images. We note that in principle wide-field SIM with sinusoidal illumination patterns can also be combined with two-photon excitation [46,47], but the very high illumination powers required and aforementioned limitations in axial resolution and imaging depth limit the advantages. A promising alternative to the approaches described above is offered by two-step excitation schemes [48]. The idea here is to use photoactivatable fluorophores [49], which are nonfluorescent until activated by blue or UV light. It is possible to structure the illumination pattern of the activation light in a similar fashion to that in wide-field SIM [50] or spot-scanning SIM [48]. This approach offers further resolution enhancements, as the cutoff frequencies of activation-, excitation-, and emission-light sum up:  $k_{2\text{step}} = k_{\text{ac}} + k_{\text{ex}} + k_{\text{em}}$ . Using this technique, the authors achieved a SIM resolution of 62 nm in live cells [50]. Although the use of two-photon excitation improves the penetration depth, the shape of the excitation spot at greater imaging depths is still subject to degradation. Furthermore, the generated fluorescence is even more strongly affected by scattering and absorption. To counteract these problems, the use of adaptive optics was introduced in microscopy. Initially, this technique was developed for astronomy applications to correct for aberrations in the atmosphere, but the same principles have been applied to correct for aberrations in microscopy. To compensate for wavefront aberrations, the illuminating beam is directed onto an adaptive optical element, for example, a spatial light modulator or a deformable mirror. The active pixels on these devices can control the phase of the light and are used to impart a wavefront distortion to the beam before it enters the sample that pre-compensates for phase distortions experienced as the beam propagates through the sample. As a result, tight focusing is possible, even in aberrating samples. Similar corrections can also be made for detected light to “undo” distortions experienced by the emitted light as it travels through the sample toward the detector [51]. Two different algorithms have been proposed to provide feedback on phase distortions, and thus to adjust the adaptive optical elements accordingly. One measures the wavefront distortions directly using a Shack–Hartmann wavefront sensor [52],

and the other is a purely computational procedure, which, through iterative optimization, provides estimates of the wavefront distortion. The latter requires no additional hardware and is applicable even in wide-field SIM [53]. Alternatively, methods have also been proposed that estimate distortions in the illumination pattern directly during the reconstruction process [54]. When these technologies are put together in a single setup, images of remarkable clarity and resolution can be generated that offer profound insights in live microscopic specimens; Fig. 5(a), for instance, shows a nematode larva imaged in two colors with an all-optical two-photon ISM system [45]. Zooming closer [Figs. 5(c) and 5(d)] reveals individual neurons expressing the transcriptional reporter protein psax-3::GFP. As the imaged animal is alive, the functional activity of neurons can be studied in real time, *in situ*, and *in vivo* with optical superresolution. In a similar fashion, zebrafish embryos can be imaged during development, as depicted in Fig. 5(g). Here a 3D rendering of the developing eye in a 40 h old live zebrafish embryo is shown at an overall resolution of well below 200 nm and an imaging depth up to 100  $\mu\text{m}$ .

These examples show that the door is now open for intravital imaging at optical superresolution, which permits the detailed study of the chemistry of life as it occurs in cells deeply buried within developing and living organisms. However, there are also enormous opportunities to study chemical processes under *in vitro* conditions using novel modalities of SIM that achieve even higher resolution than what we have hereto described. For studies *in vitro*, a novel SIM modality is currently being actively researched and developed, and it promises to achieve nanoscopic resolution comparable to rivaling techniques such as STED and SMLM: plasmonic SIM (PSIM).

#### 4. WIDE-FIELD SIM USING PLASMONIC ILLUMINATION PATTERNS

A high chemical specificity and good spatiotemporal resolution are invaluable properties for the visualization of chemical and biochemical process kinetics. Conventional SIM systems achieve two of these three characteristics, namely, specificity and temporal resolution. However, they are still restricted in terms of their achievable spatial resolution. As outlined in previous sections, the ultimate resolution achievable in SIM is determined by the spatial frequency of the excitation pattern  $k_{\text{ex}}$ , which itself is limited by optical diffraction. Nonlinear modalities of SIM are theoretically diffraction unlimited, as was proposed in 2002 [55] and later demonstrated for wide-field SIM [28,56] and spot-scanning SIM [57]. This can be understood by considering the illumination of a sample with sinusoidally modulated light patterns of very high intensity, as shown in Fig. 1. Optical transitions of sample fluorophores are more likely to be saturated in those regions where the illumination intensity is high, and thus the degree of saturation will be a function of position with respect to the illumination structure. As a result, the spatial emission pattern will no longer be purely sinusoidal, but will, in addition to the fundamental spatial frequency prescribed by the illumination pattern, also contain higher harmonics, i.e., multiples of the fundamental frequency. These higher harmonics can theoretically be used to extend the support of the OTF to arbitrarily high values. An excellent review on this topic is found in [18]. Nonlinear SIM is sometimes also treated as a RESOLFT technique (reversibly saturable, optically linear fluorescence transitions) [16]. The



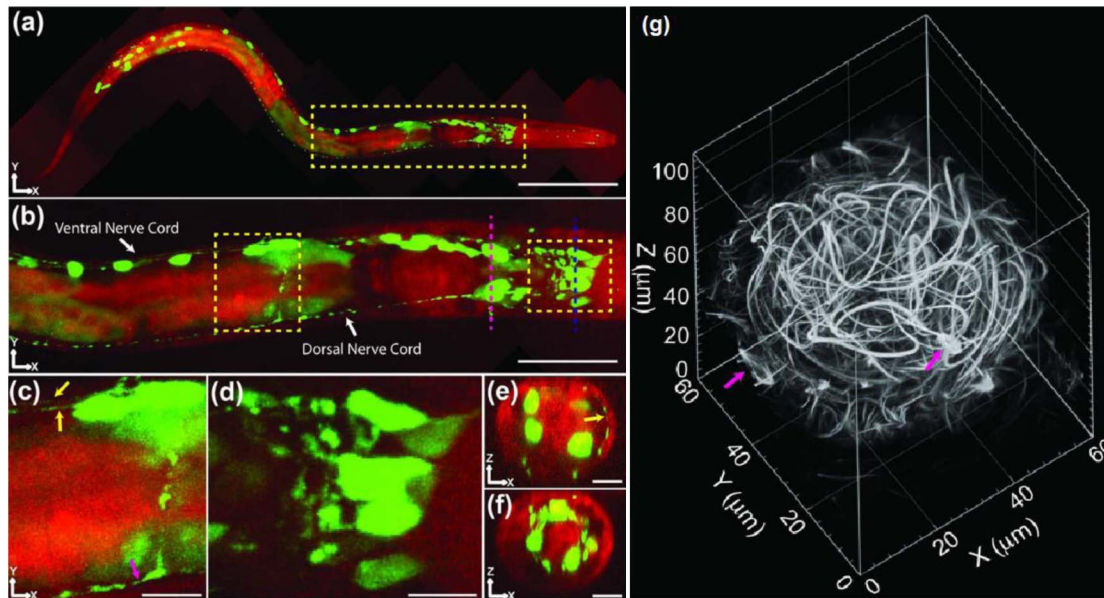


**Fig. 5.** Two-photon imaging with an all-optical ISM system. (a) Anesthetized nematode larva imaged in two colors. The larva's neurons expressing the protein GFP are clearly visible in green. The body of the larva was imaged using autofluorescence and appears red in the image. (b)–(f) Enlarged regions demonstrate the power of this technique to visualize biological processes inside live animal neurons. The yellow and magenta arrows point to fascicles of the nerve cords. (g) Eye of a 40 h old zebrafish. The images visualize the microtubule network inside the eye, and the magenta arrows point to locations where cells undergo mitosis, clearly visible from the opposing arrangement of microtubule bundles. Images reprinted from Winter *et al.* [45], with permission. Scale bars: (a) 60  $\mu\text{m}$ ; (b) 20  $\mu\text{m}$ ; (c), (d) 4  $\mu\text{m}$ ; (e), (f) 5  $\mu\text{m}$ .

big drawback of nonlinear SIM is, however, that the high illumination intensities required for saturation also induce photobleaching and associated phototoxicity. The need for high intensity in nonlinear SIM can be circumvented through a trick that makes use of optical dispersion in a linear implementation of SIM, which, like nonlinear SIM, is also theoretically unlimited in resolution. The method requires the use of surface plasmon polaritons (SPPs), which can be spatially patterned at very high frequency. Conventionally, the spatial frequency  $k$  of light is linearly dependent on its angular frequency  $\omega$ , *via* the speed of light  $c$ :

$$k = \frac{\omega}{c}. \quad (5)$$

However, it was already shown in the 1950s that light can travel along metallic surfaces at the metal–air interface [58] in the form of SPPs, and that for these surface-bound light waves, the dispersion relation in Eq. (5) no longer holds. For SPPs  $k$  depends on the dielectric functions of the metal  $\epsilon_{\text{metal}}(\omega)$  and that of the surrounding insulator  $\epsilon_{\text{insulator}}(\omega)$  in a complex fashion. The latter account for the response of the metal's electrons to the electric field variations in the light wave:

$$k_{\text{SPP}} = \frac{\omega}{c} \left( \frac{\epsilon_{\text{metal}}(\omega)\epsilon_{\text{insulator}}(\omega)}{\epsilon_{\text{metal}}(\omega) + \epsilon_{\text{insulator}}(\omega)} \right)^{1/2}. \quad (6)$$

Here  $k_{\text{SPP}}$  refers to the spatial frequency of the SPP, and its value is plotted against the angular frequency  $\omega$  in the upper panel of Fig. 6.

Clearly, the wave vector of the SPP light can reach far greater values of  $k$  than light propagating in free space; however, photon energy in the plasmon field is unchanged, and thus the resonance conditions needed to excite fluorophores remain unchanged. Furthermore, two counterpropagating SPPs can interfere with

one another and thus produce ultrafine stripe patterns that provide outstanding potential to further improve resolution in wide-field SIM approaches. Since SPPs are inherently confined to the substrate surface they are traveling on, their intensity decays within tens of nanometers perpendicular to that surface,

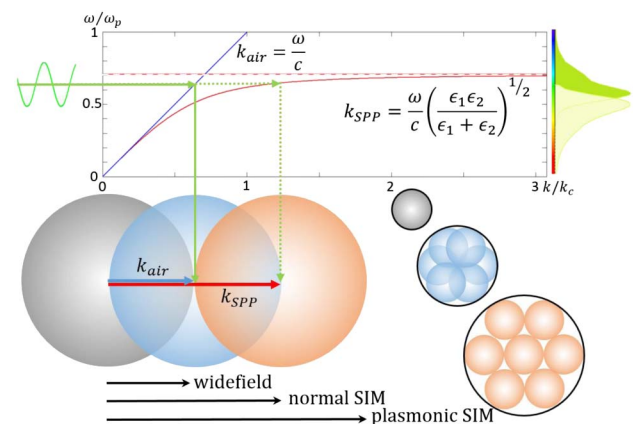


**Fig. 6.** Principle of resolution improvement in plasmonic SIM. In conventional mounting media such as air, water, or oil, the relation between the angular frequency  $\omega$  and the wave vector  $k$  of the illumination light is linear. Hence, the maximum resolution in conventional SIM, as defined by the sum frequency of illumination wave vector  $k_{\text{air}}$  and emission wave vector  $k_{\text{em}} \approx k_{\text{air}}$ , is approximately twice that of wide-field imaging. At the interface between a metal and an insulator, the dispersion relationship becomes nonlinear, due to the influence of the materials' dielectric functions  $\epsilon_1$  and  $\epsilon_2$ , which are themselves functions of  $\omega$ . It is therefore possible to generate spatial frequencies that are far beyond those permitted by the diffraction limit in conventional imaging media. Note that this is not inconsistent with Abbe theory, because plasmons are near-field phenomena and thus not constrained by diffraction.

in a fashion similar to evanescent fields in **total internal reflection fluorescence (TIRF) illumination** [59]. Consequently, the **background fluorescence** is very effectively suppressed. These features are set to make PSIM [60] an extremely powerful superresolution modality, although research in this field is still in its infancy. As a further advantage, in certain implementations of PSIM, the excitation fringe pattern can be generated with **a single beam** using appropriately structured metal films. The principle is shown in Fig. 7, where a **metal-coated coverslip** is prepared with **periodically arranged slits** along the surface. This allows the illumination light to be coupled into the metal coating such that the SPPs generate standing waves upon reflection at the metal boundaries, as illustrated in Fig. 7. Note that for efficient coupling, the angle of incidence has to be close to the **SPP coupling angle  $\theta_{\text{SPP}}$**  (see next paragraph for a discussion). Plasmon waves are then launched in both directions starting from the slits and can **interfere with plasmon waves from neighboring slits** to produce diffraction-unlimited fringe patterns. To change the starting phase of the standing wave, it suffices to make **small adjustments to the incident angle of the illumination light** [60].

The overall setup of a PSIM microscope is essentially that of a conventional TIRF microscope [61]; the main difference lies in the requirement for a **special coating** on the coverslip. The post-processing of PSIM data is, however, much more challenging than for conventional SIM. In practice, the coating material must be chosen appropriately for the particular application, as the acceptance angle  $\theta_{\text{SPP}}$  is **material dependent** and can vary from  $\sim 45^\circ$  for gold coatings to  $\sim 70^\circ$  for a silver–water interface [62]. As **silver coatings support SPPs at visible wavelengths**, it is likely to become the material of choice for many future PSIM implementations. We note that **only *p*-polarized light** can be launched into plasmonic waves. It has already been used to demonstrate **a resolution increase of 2.6** [60], and could become the next generation of TIRF-SIM, which already achieves a  $2.1 \times$  resolution improvement to about 90 nm [29,50]. Simulations of **graphene-coated coverslips** even promise a resolution improvement down into **the range of several tens of nanometers** [63].

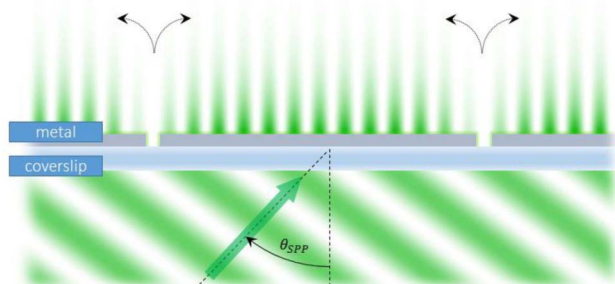


**Fig. 7.** Pattern generation in plasmonic SIM (PSIM). In contrast to conventional SIM, only **a single illumination beam** is required in PSIM. A plasmonic standing wave pattern can be created with a single wave incident on a metal coated coverslip, featuring tiny slits that are periodically distributed on the surface on a micrometer scale [60]. The angle of incidence of the excitation light is as close as possible to the SPP acceptance angle  $\theta_{\text{SPP}}$ . Due to the slits, the illumination light can couple into the coating and travel along the surface in both directions from the slit. The interference of two counterpropagating SPPs thus creates a fringe pattern with spatial frequency  $k_{\text{SPP}}$  that is beyond the cutoff frequency of conventional SIM.

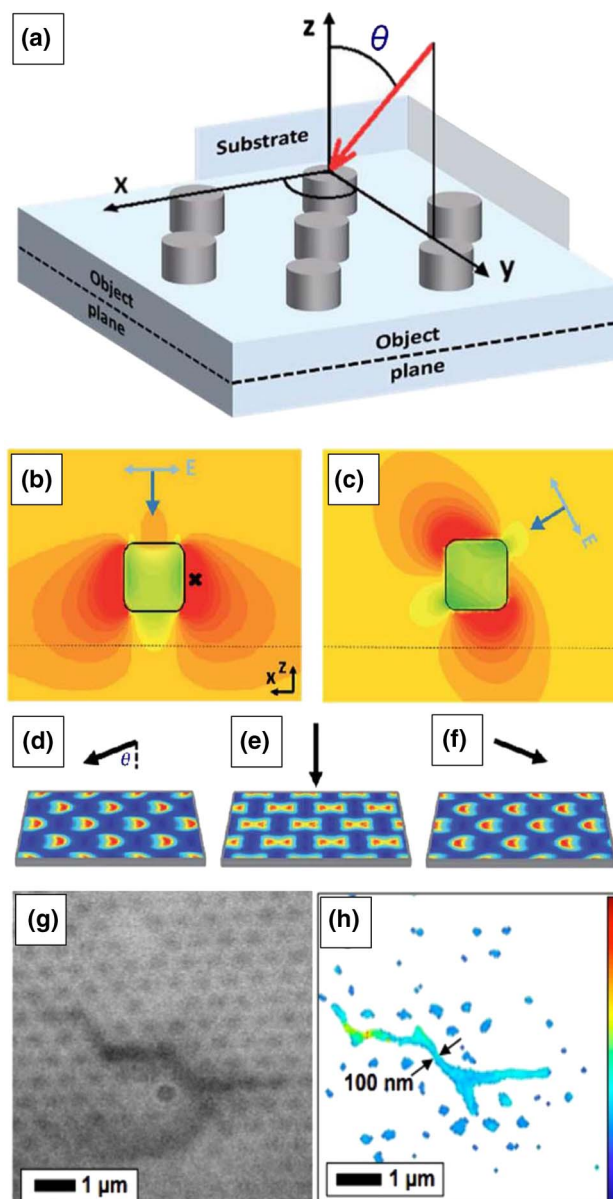


**Fig. 8.** Pattern generation in localized plasmon SIM (LPSIM). (a) Light from a single beam incident on a nanostructured substrate creates localized plasmon resonances with dimensions below the diffraction limit. Note that the angle of incidence  $\theta$  is not critical in generating localized plasmons and can be very different from the acceptance angle  $\theta_{\text{SPP}}$  required for PSIM (see Fig. 7). However, the shape of the localized plasmon field pattern is strongly dependent on  $\theta$ , as shown in (b)–(f), and can thus be as a method to induce “pattern shifts” as required for the reconstruction of superresolved images from the raw data. In this configuration the limiting factor is not the diffraction of light but **the precision at which nanostructures and field patterns can be produced**. Images in (a)–(f) are adapted from Ponsetto *et al.* [65] with permission of The Royal Society of Chemistry. LPSIM is compatible also with **marker-free imaging** and could be combined with surface enhanced Raman spectroscopy (SERS) [67]. That this is, in principle, possible is shown in (g), which represents an optical micrograph of a collagen fibril, and (h), the respective superresolved LPSIM-SERS image. The color scale represents the relative intensity of the detected signal. Images in (g), (h) reprinted with permission from C. T. Ertsgaard, R. M. Mckoskey, I. S. Rich, and N. C. Lindquist, “Dynamic Placement of Plasmonic Hotspots for Super-Resolution Surface-Enhanced Raman Scattering,” *ACS Nano* **8**, 10941–10946 (2014). Copyright (2014) American Chemical Society.



There is another method for the implementation of PSIM that makes use of localized plasmons (LPs) excited near nanostructures periodically placed directly on the coverslip. These can be made of, e.g., glass [64], silver [65], or gold [66]. The corresponding technique has been named LPSIM [65]. Here, it is not the frequency of the illumination light that determines the spatial frequency of the periodic plasmon intensity distribution, but solely the spatial period of the nanostructure pattern situated on the coverslip. An example for such a nanostructured pattern is shown in Fig. 8. Here, tiny metal disks are placed in a honeycomb pattern on a substrate, with distances between neighboring disks far smaller than the diffraction limit to capture and convert incident light into LPs. In this approach the angle of incidence is not a constraining factor, which is in contrast to PSIM. Instead, the launch angle can be varied to produce “phase shifted” patterns as required for the reconstruction process [see Figs. 8(b)–8(f)].

The light that is bound to the disks is a near-field phenomenon and only penetrates into the sample for a depth of several tens of nanometers, i.e., offering the same intrinsic contrast afforded by PSIM and TIRF microscopy. Additionally, the nanostructures can theoretically be tailored for use with any illumination wavelength and therefore permit the use of many biochemically interesting dyes. Furthermore, concepts that combine LPSIM with interfering beams for illumination have been discussed and could provide further improvements in resolution by gaining extra spatial information from combinations of  $k$ -vectors that reflect periodicities in both the nanostructures on the substrate and the intensity pattern of the light [64,66]. This is conceptually analogous to the discussion around Fig. 6. So far PSIM and LPSIM both have only been studied in simulations and in basic experimental demonstrations with fluorescent beads. Nevertheless, these early results promise an interesting future for these techniques in dynamic *in vitro* imaging applications that require nanoscale resolution. This could be especially true if they are combined with two-step excitation methods, which double the effective spatial frequency in the illumination pattern [48]. LPSIM can even be used as a label-free imaging method: in combination with surface-enhanced Raman spectroscopy, superresolution is obtained with molecular specificity without a requirement for fluorescent labels [67]. An early demonstration is shown in Fig. 8(h), where collagen fibrils are imaged at 100 nm resolution, without use of labels. In conclusion, these new SIM modalities, spot-scanning SIM and PSIM, are likely to push the technique beyond the current resolution boundaries. A comparison of SIM with plasmonic illumination and spot-scanning SIM is shown in Table 1. While spot-scanning SIM techniques are most useful for the study of biochemical processes in living environments, PSIM

has the potential to become the method of choice for real-time nanoscopic imaging of molecular phenomena *in vitro*.

## 5. SUMMARY

Two novel modalities of SIM imaging have been explored in this review, variants of which hold promise for further step changes in the application of optical imaging in biomedical and chemical research. The first concerns the so-called spot-scanning implementations of SIM and their parallelized variants, called MSIM. These techniques can be combined with two-photon excitation and adaptive optics, which have opened up the field of SIM imaging for intravital applications and which enable studies of chemical processes deep inside live and developing organisms at unprecedented resolutions and frame rates. The second major innovation lies in the use of plasmonic structures in wide-field implementations of SIM, which will permit the imaging of chemical species *in vitro* with theoretically unlimited resolutions at high speed. Since plasmonic excitation fields are surface-bound, these techniques avoid the generation of out-of-focus signals, similar to TIRF-SIM, thus greatly improving contrast. Due to a nonlinear dispersion relation between illumination frequency and the SPP wave vector, standing plasmon resonances have the potential to offer considerable resolution improvements. In the future this could be used to “capture movies” of dynamic chemical processes in real time.

Nevertheless, SIM should not be seen as a standalone technology, as its principle can also be applied quite generally in combination with other imaging modalities. Breathtaking images were recently presented by Chen *et al.*, who demonstrated a technique called lattice SIM [27], which combines the low phototoxicity and imaging speed of selective plane illumination microscopy with the resolution doubling potential of SIM. Combinations with other superresolution modalities are also conceivable and could provide synergistic effects. Correlative imaging of STORM and SIM was already proposed and implemented [68,69] to cross-validate the two methods and to correct for reconstruction artifacts specific to each of the two techniques. It may also be useful in future setups to not only overlay the images from different modalities but also combine and process respective raw data to yield a superior data set that bridges resolution gaps and reveals yet further detail, thus “combining the best of several imaging worlds.” In STED microscopy, higher acquisition speeds might be achievable than are currently possible *via* a combination with PSIM [70]. Other approaches might take into account the structured illumination character of parallelized STED [71] and treat corresponding data with MSIM reconstruction algorithms [38], thus exploiting the resolving power of STED and SIM to their full combined potential.

**Table 1. Comparison of Spot-Scanning SIM and Plasmonic Wide-Field SIM**

Spot-Scanning SIM	Plasmonic Wide-Field SIM
+ Penetration depth	+ “Unlimited” resolution
+ Two-photon illumination	+ High contrast
+ Axial superresolution	+ High-speed imaging
+ Adaptive optics	– Requires special coverslips
+ All-optical processing	– Reconstruction methods challenging
– Only doubled resolution	– Restricted imaging depth

**Funding.** Leverhulme Trust (RPG-2012-793); Engineering and Physical Sciences Research Council (EPSRC) (EP/H018301/1); Medical Research Council (MRC) (MR/K015850/1, MR/K02292X/1); Wellcome Trust (089703/Z/09/Z); Alzheimer’s Research UK (ARUK) (ARUK-EG2012A-1).

## REFERENCES

1. S. Hell and J. Wichmann, “Breaking the diffraction resolution limit by stimulated emission: stimulated-emission-depletion fluorescence microscopy,” *Opt. Lett.* **19**, 780–782 (1994).

2. W. Moerner and L. Kador, "Optical detection and spectroscopy of single molecules in a solid," *Phys. Rev. Lett.* **62**, 2535–2538 (1989).
3. E. Betzig, "Proposed method for molecular optical imaging," *Opt. Lett.* **20**, 237–239 (1995).
4. E. Abbe, "Beiträge zur theorie des mikroskops und der mikroskopischen wahrnehmung," *Archiv f. Mikr. Anat.* **9**, 413–418 (1873).
5. L. Rayleigh, "XV. On the theory of optical images, with special reference to the microscope," *Philos. Mag. Ser. 5* **42**(255), 167–195 (1896).
6. K. Lidke, B. Rieger, T. Jovin, and R. Heintzmann, "Superresolution by localization of quantum dots using blinking statistics," *Opt. Express* **13**, 7052–7062 (2005).
7. E. Betzig, G. H. Patterson, R. Sougrat, O. W. Lindwasser, S. Olenych, J. S. Bonifacio, M. W. Davidson, J. Lippincott-Schwartz, and H. F. Hess, "Imaging intracellular fluorescent proteins at nanometer resolution," *Science* **313**, 1642–1645 (2006).
8. S. T. Hess, T. P. K. Girirajan, and M. D. Mason, "Ultra-high resolution imaging by fluorescence photoactivation localization microscopy," *Biophys. J.* **91**, 4258–4272 (2006).
9. M. Rust, M. Bates, and X. Zhuang, "Sub-diffraction-limit imaging by stochastic optical reconstruction microscopy (STORM)," *Nat. Methods* **3**, 793–796 (2006).
10. M. Heilemann, S. Van De Linde, M. Schüttel, R. Kasper, B. Seefeldt, A. Mukherjee, P. Tinnefeld, and M. Sauer, "Subdiffraction-resolution fluorescence imaging with conventional fluorescent probes," *Angew. Chem. Int. Ed.* **47**, 6172–6176 (2008).
11. J. Fölling, M. Bossi, H. Bock, R. Medda, C. A. Wurm, B. Hein, S. Jakobs, C. Eggeling, and S. W. Hell, "Fluorescence nanoscopy by ground-state depletion and single-molecule return," *Nat. Methods* **5**, 943–945 (2008).
12. C. J. R. Sheppard, "Super-resolution in confocal imaging," *Optik* **80**, 53–54 (1988).
13. R. Heintzmann and C. Cremer, "Laterally modulated excitation microscopy: improvement of resolution by using a diffraction grating," *Proc. SPIE* **3568**, 185–196 (1999).
14. M. Gustafsson, "Surpassing the lateral resolution limit by a factor of two using structured illumination microscopy," *J. Microsc.* **198**, 82–87 (2000).
15. J. Lippincott-Schwartz and S. Manley, "Putting super-resolution fluorescence microscopy to work," *Nat. Methods* **6**, 21–23 (2009).
16. S. Hell, "Far-field optical nanoscopy," *Science* **316**, 1153–1158 (2007).
17. L. Schermelleh, R. Heintzmann, and H. Leonhardt, "A guide to super-resolution fluorescence microscopy," *J. Cell Biol.* **190**, 165–175 (2010).
18. R. Heintzmann and M. Gustafsson, "Subdiffraction resolution in continuous samples," *Nat. Photonics* **3**, 362–364 (2009).
19. J. R. Allen, S. T. Ross, and M. W. Davidson, "Structured illumination microscopy for superresolution," *Chem. Phys. Chem.* **15**, 566–576 (2014).
20. A. Jost and R. Heintzmann, "Superresolution multidimensional imaging with structured illumination microscopy," *Ann. Rev. Mater. Res.* **43**, 261–282 (2013).
21. K. Wicker, "Super-resolution fluorescence microscopy using structured illumination," in *Super-Resolution Microscopy Techniques in the Neurosciences*, E. F. Fornasiero and S. O. Rizzoli, eds., Neuromethods Series (Humana, 2014), pp. 133–166.
22. P. W. Winter and H. Shroff, "Faster fluorescence microscopy: advances in high speed biological imaging," *Curr. Opin. Chem. Biol.* **20**, 46–53 (2014).
23. R. Fiolka, "Three-dimensional live microscopy beyond the diffraction limit," *J. Opt.* **15**, 094002 (2013).
24. G. Ball, R. M. Parton, R. S. Hamilton, and I. Davis, *A Cell Biologist's Guide to High Resolution Imaging*, 1st ed. (Elsevier, 2012), Vol. **504**.
25. R. Han, Z. Li, Y. Fan, and Y. Jiang, "Recent advances in super-resolution fluorescence imaging and its applications in biology," *J. Genet. Genomics* **40**, 583–595 (2013).
26. Y. Wu, R. Christensen, D. Colón-Ramos, and H. Shroff, "Advanced optical imaging techniques for neurodevelopment," *Curr. Opin. Neurobiol.* **23**, 1090–1097 (2013).
27. B.-C. Chen, W. R. Legant, K. Wang, L. Shao, D. E. Milkie, W. Michael, C. Janetopoulos, X. S. Wu, J. A. H. Iii, Z. Liu, B. P. English, Y. Mimori-Kiyosue, D. P. Romero, A. T. Ritter, J. Lippincott-Schwartz, R. D. Mullins, D. M. Mitchell, J. N. Bembenek, R. Böhme, S. W. Grill, J. T. Wang, G. Seydoux, U. Serdar, D. P. Kiehart, and E. Betzig, "Lattice light sheet microscopy: imaging molecules, cells, and embryos at high spatiotemporal resolution," *Science* **346**, 1257998 (2014).
28. M. Gustafsson, "Nonlinear structured-illumination microscopy: wide-field fluorescence imaging with theoretically unlimited resolution," *Proc. Natl. Acad. Sci. USA* **102**, 13081–13086 (2005).
29. R. Fiolka, M. Beck, and A. Stemmer, "Structured illumination in total internal reflection fluorescence microscopy using a spatial light modulator," *Opt. Lett.* **33**, 1629–1631 (2008).
30. M. Gustafsson, L. Shao, and P. Carlton, "Three-dimensional resolution doubling in wide-field fluorescence microscopy by structured illumination," *Biophys. J.* **94**, 4957–4970 (2008).
31. L. Shao, B. Isaac, S. Uzawa, D. A. Agard, J. W. Sedat, and M. G. L. Gustafsson, "iLS: wide-field light microscopy with 100-nm-scale resolution in three dimensions," *Biophys. J.* **94**, 4971–4983 (2008).
32. C. J. Sheppard and T. Wilson, "The theory of the direct-view confocal microscope," *J. Microsc.* **124**, 107–117 (1981).
33. C. B. Müller and J. Enderlein, "Image scanning microscopy," *Phys. Rev. Lett.* **104**, 198101 (2010).
34. A. G. York, P. Chandris, D. D. Nogare, J. Head, P. Wawrzus, R. S. Fischer, A. Chitnis, and H. Shroff, "Instant super-resolution imaging in live cells and embryos via analog image processing," *Nat. Methods* **10**, 1122–1126 (2013).
35. C. J. R. Sheppard, S. B. Mehta, and R. Heintzmann, "Superresolution by image scanning microscopy using pixel reassignment," *Opt. Lett.* **38**, 2889–2892 (2013).
36. O. Schulz, C. Pieper, M. Clever, J. Pfaff, A. Ruhlandt, R. H. Kehlenbach, F. S. Wouters, J. Großhans, G. Bunt, and J. Enderlein, "Resolution doubling in fluorescence microscopy with confocal spinning-disk image scanning microscopy," *Proc. Natl. Acad. Sci. USA* **110**, 21000–21005 (2013).
37. A. G. York, S. H. Parekh, D. Dalle Nogare, R. S. Fischer, K. Temprine, M. Mione, A. B. Chitnis, C. A. Combs, and H. Shroff, "Resolution doubling in live, multicellular organisms via multifocal structured illumination microscopy," *Nat. Methods* **9**, 749–754 (2012).
38. F. Ströhl and C. F. Kaminski, "A joint Richardson–Lucy deconvolution algorithm for the reconstruction of multifocal structured illumination microscopy data," *Methods Appl. Fluoresc.* **3**, 014002 (2015).
39. G. M. R. De Luca, R. M. P. Breedijk, R. A. J. Brandt, C. H. C. Zeelenberg, B. E. de Jong, W. Timmermans, L. N. Azar, R. A. Hoebe, S. Stallinga, and E. M. M. Manders, "Re-scan confocal microscopy: scanning twice for better resolution," *Biomed. Opt. Express* **4**, 2644–2656 (2013).
40. S. Roth, C. J. Sheppard, K. Wicker, and R. Heintzmann, "Optical photon reassignment microscopy (OPRA)," *Opt. Nanoscopy* **2**, 5 (2013).
41. J. Huff, "The Airyscan detector from ZEISS: confocal imaging with improved signal-to-noise ratio and super-resolution," *Nat. Methods* **12**, i–ii (2015).
42. T. Azuma and T. Kei, "Super-resolution spinning-disk confocal microscopy using optical photon reassignment," *Opt. Express* **23**, 15003–15011 (2015).
43. W. Denk, J. H. Strickler, and W. W. Webb, "Two-photon laser scanning fluorescence microscopy," *Science* **248**, 73–76 (1990).
44. M. Ingaramo, A. G. York, P. Wawrzus, O. Milberg, A. Hong, R. Weigert, H. Shroff, and G. H. Patterson, "Two-photon excitation improves multifocal structured illumination microscopy in thick scattering tissue," *Proc. Natl. Acad. Sci. USA* **111**, 5254–5259 (2014).
45. P. W. Winter, A. G. York, D. D. Nogare, M. Ingaramo, R. Christensen, A. Chitnis, G. H. Patterson, and H. Shroff, "Two-photon instant structured illumination microscopy improves the depth penetration of super-resolution imaging in thick scattering samples," *Optica* **1**, 181–191 (2014).
46. V. Andresen, K. Pollok, and J. Rinnenthal, "High-resolution intravital microscopy," *PLoS ONE* **7**, e50915 (2012).
47. L.-C. Cheng, C.-H. Lien, Y. Da Sie, Y. Y. Hu, C.-Y. Lin, F.-C. Chien, C. Xu, C. Y. Dong, and S.-J. Chen, "Nonlinear structured-illumination enhanced temporal focusing multiphoton excitation microscopy with a digital micromirror device," *Biomed. Opt. Express* **5**, 2526–2536 (2014).
48. M. Ingaramo, A. G. York, E. J. Andrade, K. Rainey, and G. H. Patterson, "Two-photon-like microscopy with orders-of-magnitude lower illumination intensity via two-step fluorescence," *Nat. Commun.* **6**, 8184 (2015).
49. D. M. Shcherbakova, P. Sengupta, J. Lippincott-Schwartz, and V. V. Verkhusha, "Photocontrollable fluorescent proteins for superresolution imaging," *Ann. Rev. Biophys.* **43**, 303–329 (2014).
50. D. Li, L. Shao, B.-C. Chen, X. Zhang, M. Zhang, B. Moses, D. E. Milkie, J. R. Beach, J. A. Hammer, M. Pasham, T. Kirchhausen, M. A. Baird, M. W. Davidson, P. Xu, and E. Betzig, "Extended-resolution structured

- illumination imaging of endocytic and cytoskeletal dynamics," *Science* **349**, aab3500 (2015).
51. M. J. Booth, "Adaptive optics in microscopy," *Philos. Trans. Ser. A* **365**, 2829–2843 (2007).
  52. X. Tao, B. Fernandez, O. Azucena, M. Fu, D. Garcia, Y. Zuo, D. C. Chen, and J. Kubby, "Adaptive optics confocal microscopy using direct wave-front sensing," *Opt. Lett.* **36**, 1062–1064 (2011).
  53. B. Thomas, A. Wolstenholme, S. N. Chaudhari, E. T. Kipreos, and P. Kner, "Enhanced resolution through thick tissue with structured illumination and adaptive optics," *J. Biomed. Opt.* **20**, 026006 (2015).
  54. R. Ayuk, H. Giovannini, A. Jost, E. Mudry, J. Girard, T. Mangeat, N. Sandeau, R. Heintzmann, K. Wicker, K. Belkebir, and A. Sentenac, "Structured illumination fluorescence microscopy with distorted excitations using a filtered blind-SIM algorithm," *Opt. Lett.* **38**, 4723–4726 (2013).
  55. R. Heintzmann, T. M. Jovin, and C. Cremer, "Saturated patterned excitation microscopy: a concept for optical resolution improvement," *J. Opt. Soc. Am. A* **19**, 1599–1609 (2002).
  56. E. H. Rego, L. Shao, J. J. Macklin, L. Winoto, G. A. Johansson, N. Kamps-Hughes, M. W. Davidson, and M. G. L. Gustafsson, "PNAS plus: nonlinear structured-illumination microscopy with a photoswitchable protein reveals cellular structures at 50-nm resolution," *Proc. Natl. Acad. Sci. USA* **109**, E135–E143 (2012).
  57. G. P. J. Laporte, N. Stasio, C. J. R. Sheppard, and D. Psaltis, "Resolution enhancement in nonlinear scanning microscopy through post-detection digital computation," *Optica* **1**, 455–460 (2014).
  58. R. Ritchie, "Plasma losses by fast electrons in thin films," *Phys. Rev.* **106**, 874–881 (1957).
  59. E. Chung, D. Kim, and P. So, "Extended resolution wide-field optical imaging: objective-launched standing-wave total internal reflection fluorescence microscopy," *Opt. Lett.* **31**, 945–947 (2006).
  60. F. Wei, D. Lu, H. Shen, W. Wan, J. L. Ponsetto, E. Huang, and Z. Liu, "Wide field super-resolution surface imaging through plasmonic structured illumination microscopy," *Nano Lett.* **14**, 4634–4639 (2014).
  61. L. J. Young, F. Ströhl, and C. F. Kaminski, "A guide to structured illumination TIRF microscopy at high speed with multiple colors," 2016, <https://www.repository.cam.ac.uk/handle/1810/252608>.
  62. E. Chung, Y.-H. Kim, W. T. Tang, C. J. R. Sheppard, and P. T. C. So, "Surface-plasmon-resonance waves," *Opt. Lett.* **34**, 2366–2368 (2009).
  63. X. Zeng and M. S. Zubairy, "Nanometer-scale microscopy via graphene plasmons," *Phys. Rev. B* **90**, 235418 (2014).
  64. A. Sentenac, K. Belkebir, H. Giovannini, and P. C. Chaumet, "High-resolution total-internal-reflection fluorescence microscopy using periodically nanostructured glass slides," *J. Opt. Soc. Am. A* **26**, 2550–2557 (2009).
  65. J. L. Ponsetto, F. Wei, and Z. Liu, "Localized plasmon assisted structured illumination microscopy for wide-field high-speed dispersion-independent super resolution imaging," *Nanoscale* **6**, 5807–5812 (2014).
  66. S. Liu, C.-J. Chuang, C. W. See, G. Zorinants, W. L. Barnes, and M. G. Somekh, "Double-grating-structured light microscopy using plasmonic nanoparticle arrays," *Opt. Lett.* **34**, 1255–1257 (2009).
  67. C. T. Ertsgaard, R. M. Mckoskey, I. S. Rich, and N. C. Lindquist, "Dynamic placement of plasmonic hotspots for super-resolution surface-enhanced Raman scattering," *ACS Nano* **8**, 10941–10946 (2014).
  68. S. Rossberger, G. Best, D. Baddeley, R. Heintzmann, U. Birk, S. Dithmar, and C. Cremer, "Combination of structured illumination and single molecule localization microscopy in one setup," *J. Opt.* **15**, 094003 (2013).
  69. V. Hamel, P. Guichard, M. Fournier, R. Guiet, I. Flückiger, A. Seitz, and P. Gönczy, "Correlative multicolor 3D SIM and STORM microscopy," *Biomed. Opt. Express* **5**, 3326–3336 (2014).
  70. H. Zhang, M. Zhao, and L. Peng, "Nonlinear structured illumination microscopy by surface plasmon enhanced stimulated emission depletion," *Opt. Express* **19**, 24783–24794 (2011).
  71. A. Chmyrov, J. Keller, T. Grotjohann, M. Ratz, E. D'Este, S. Jakobs, C. Eggeling, and S. W. Hell, "Nanoscopy with more than 100,000 'doughnuts'," *Nat. Methods* **10**, 737–740 (2013).